RSC Advances

ROYAL SOCIETY OF CHEMISTRY

www.rsc.org/advances

Cite this: DOI: 10.1039/c0xx00000x

www.rsc.org/xxxxxx

Paper

Intrinsically conducting polyaminoanthraquinone nanofibrils: Interfacial synthesis, formation mechanism and lead adsorbents†

Shao-Jun Huang,*[a] Chun-Gang Min,[a] Yaozu Liao,*[b,d] Ping Du,[a] Hui Sun,[a] Yan-Qin Zhu[a] and Ai-Min Ren[c]

Received (in XXX, XXX) Xth XXXXXXXXX 20XX, Accepted Xth XXXXXXXXX 20XX
DOI: 10.1039/b000000x

Intrinsically conducting nanofibrils of poly(1-amino-5-chloroanthraquinone) (PACA) were successfully synthesized *via* interfacial chemical oxidative polymerization of 1-amino-5-chloroanthraquinone (ACA) monomers in biphasic systems. The effects of reaction parameters including polymerization media and temperatures, oxidant species, monomer concentrations, oxidant/monomer molar ratios and acid concentrations on the polymerization yield, bulk electrical conductivity, diameters and aspect ratio of resulting PACA nanofibrils were systematically optimized. PACA nanofibrils exhibit the highest polymerization yield of 64.8%, aspect ratio of 67 (~ 30 nm of diameter, ~ 2 μm of length) and bulk electrical conductivity of 6.2×10^{-3} S/cm, when the ACA monomers were oxidized by CrO_3 in a combined medium consisting of nitrobenzene and 250 mmol/L $HClO_4$ solution. PACA nanofibrils are highly water-dispersible and self-stable with no need adding of any stabilizers. The formation mechanism of PACA nanofibrils was explored to understand what contributions are responsible for the functionalities. With clean surface, high negatively charged density and thermostability as well as strong blue-light emitting fluorescence property, PACA nanofibrils are very promising materials for fabrication of advanced iron sensors and lead adsorbents.

1. Introduction

Over two decades, conducting polymers made from heterocyclic and/or polycyclic aromatic hydrocarbons (PAHs) functionalized with amino, hydroxyl, vinyl and sulfonate groups have attracted much attention because of their promising applications for catalysts,[1–6] sensors,[7–10] electrical or optoelectronic devices[11,12] and heavy metal ion adsorbents.[13] Chemical oxidative polymerization is believed to be an effective method to synthesize such useful conducting polymers associating with high yield, simple doping/dedoping chemistry and controllable morphology can be obtained on products.[14–16] Many PAHs including aminoquinoline, diaminonaphthalene and diaminocarbazole have been reported to synthesize corresponding conducting polymers using chemical oxidative polymerization method.[17–20] Interestingly, a well-known and commercially available PAH, aminoanthraquinone (AQ) and its derivatives have been rarely studied to make conducting polymers. This is most likely that no solvents are able to dissolve the AQ monomers and oxidants well simultaneously. Common oxidants such as ammonium persulfate, ferric chloride, potassium chromate and sodium hypochlorite are usually soluble in aqueous solution while the AQ monomers are only soluble in high polar organic solvents. Even a small amount of water significantly reduces the solubility of the monomers and as-formed oligomers during polymerization and speeds the precipitation of oligomers, thereby terminating the growth of polymer chains. Finally, low molecular weight of polyaminoanthraquinone (PAQ) is obtained. For example, Huang *et al*. reported that polysulfoaminoanthraquinone (PSA) created in a single-phase of acidic aqueous medium has only 2–4 of polymerization degree.[21] In the meantime, the PAQ[22,23] and its derivative poly(1,5-diamino-anthraquinone) (PDAQ)[24] have been reported as form of agglomerates. To the best of our knowledge, highly ordered and water-dispersible polyaminoanthraquinone nanofibrils have never been reported yet.

Interfacial polymerization of PAHs demonstrates many advantages over homogeneous polymerization. Firstly, major drawbacks confronting homogeneous polymerization, especially for AQ monomers, are unable to control morphology (polymers are generally granular in morphology because of overgrowth or secondary growth) and low crystallinity of product is usually obtained.[22–24] Interfacial polymerization represents an effective method of suppressing the overgrowth or secondary growth of polymers and has been successfully applied to make polyaniline nanofibers and nanoparticles.[15,25–27] Secondly, in case of homogeneous polymerization, there is a restriction in selection of the oxidizing agents due to non-solubility of oxidizing agents and monomers in the same solvent. This problem aggravates in case of polymerization of PAHs as they are generally insoluble in all aqueous media. Interfacial polymerization avoids using single solvent which must dissolve both oxidizing agent and monomer. One can use a biphasic medium consisting of organic solvent and

aqueous acid or water alone to dissolve the monomer and oxidant, respectively. Thirdly, interfacial polymerization also enables us to synthesize various morphologies such as nanorods, nanotubes, nanosheets, nanospheres and nanofibers.[26,28–30] Typical examples are one-dimensional nanotubes and three-dimensional nanospheres of polyaniline and polypyrrole.[31–34] Besides, the post-treatments of interfacial polymerization, such as removal of residual oxidant from the products, are easy to operate because major residual oxidant is present in a single phase.

In this work, high molecular weight of PAQ derivative, poly(1-amino-5-chloroanthraquinone) (PACA) nanofibrils were simply synthesized through interfacial chemical oxidative polymerization of 1-amino-5-chloroanthraquinone (ACA) monomer in presence of a biphasic medium consisting of organic solvent and aqueous acid or water alone. The polymerization yields, chemical structures, morphology, thermal stability, fluorescence and electrical conductivity of the as-formed PACA nanofibrils were optimized by careful choice of the reaction parameters including polymerization media and temperatures, oxidant species, monomer concentrations, oxidant/monomer ratios and acid concentrations. The successful building up the PACA nanofibrils with multifunctionality was confirmed by ultraviolet-visible (UV-vis), Fourier transform infrared (FT-IR), matrix-assisted laser desorption/ionization / time-of-flight (MALDI/TOF) mass, fluorescence and X-ray diffraction spectrometers, transmission electron microscopy (TEM) and thermogravimetric analysis (TGA). The formation mechanism of PACA nanofibrils was explored to understand what factors contribute the corresponding microstructures and properties. With water-dispersibility, high ordered nanostructures, tunable electrical conductivity, high thermostability and strong blue light-emitting fluorescence property, PACA nanofbrils hold promising applications for heavy metal ion sensors and adsorbents.

2. Experimental section

2.1 Chemicals

1-Amino-5-chloroanthraquinone (ACA), chromium trioxide (CrO_3), sodium hypochlorite (NaClO), ammonium persulfate (APS, $(NH_4)_2S_2O_8$), ferric chloride ($FeCl_3$), potassium chromate (K_2CrO_4), lead nitrate ($Pb(NO_3)_2$), perchloric acid ($HClO_4$), nitrobenzene ($C_6H_5NO_2$), *o*-dichlorobenzene ($C_6H_4Cl_2$), nitromethane (CH_3NO_2), chloroform ($CHCl_3$), *N*,*N*-dimethylformamide (DMF), dimethyl sulfoxide (DMSO), ethyl acetate ($MeCO_2Et$), *N*-methy1-2-pyrrolidone (NMP) and other chemicals were purchased from Chemical Reagent Corp., China. All reagents and solvents were of analytical reagent grade and used as received.

2.2 Synthesis of PACA nanofibrils

In a typical synthesis, a 100 mL conical flask was charged with 1.29 g (5.0 mmol) of ACA, 750 μL (8.8 mmol) of 70% $HClO_4$ and 30 mL of $C_6H_5NO_2$ in a water bath at 30 °C. The mixture was stirred vigorously for 20 min. An oxidant solution was prepared separately by dissolving 1.00 g (10 mmol) of CrO_3 oxidant in 5.0 mL of distilled water at 30 °C. The CrO_3 oxidant solution was then one-off added into the ACA mixing solution. The obtained mixture was magnetically stirred with a speed of 300 rpm for 72 h at 30 °C. Subsequently, the reaction mixture was separated with a 50 mL separatory funnel to give an aqueous layer and an organic layer. The aqueous layer was treated with 1 mL of absolute ethanol so that the residual toxic hexavalent chromium would turn into safe trivalent chromium. The organic layer was distilled under reduced pressure at 95 °C to give a solid product and initial $C_6H_5NO_2$. The $C_6H_5NO_2$ was recycled after dried with anhydrous calcium chloride and then redistilled. The solid product was washed with excess distilled water (2000 mL) and alcohol (300 mL) in order to remove the water soluble byproducts, remaining monomers and some oligomers, and finally dried at 80 °C in air for 2 days affording virgin doped PACA nanofibril salts. After treated by 0.2 mol/L ammonia solution (NH_4OH), the dedoped PACA nanofibrils were obtained, then treated by 1.0 mol/L $HClO_4$ again producing redoped PACA nanofibrils.

2.3 Characterization and measurements of PACA nanofibrils

The open-circuit potential (OCP) of ACA solutions was measured by PHS-3C precision acidimeter using an Ag/AgCl electrode as the inner reference electrode. The Fourier transform infrared (FT-IR) spectra were recorded on a Bruker TENSOR 27 FT-IR spectrometer with a resolution of 4 cm^{-1} by transmittance method with pressing KBr troche. The ultraviolet visible (UV−vis) spectra of obtained polymers were recorded on a TU−1901 UV−vis spectrophotometer (Beijing Purkinje General Instrument Co., Ltd.) in a wavelength range of 190−900 nm at a scanning rate of 400 nm/min. The wide-angle X-ray diffraction (WAXD) scanning was carried on a Rigaku International Corporation D/MAX-2000 X-ray diffractometer with Cu Kα radiation at a scanning rate of 10°/min. The matrix-assisted laser desorption/ionization / time-of-flight (MALDI/TOF) mass spectra of PACA in THF using 2,5-dihydroxybenzoicacid (DHB) as a matrix were recorded on a Bruker Daltonik GmbH auto flex speed TOF/TOF mass spectrometer. The fluorescence excitation and emission spectra were obtained by a PerkinElmer LS50B luminescence spectrometer. The morphology of the resulting PACA nanofibrils bundles were analyzed by a Netherlands EM420 Phillips transmission electron microscope (TEM). The size and size distribution of the PACA particles dispersed in water were analyzed by a Beckman Coulter LS230 laser particle-size analyzer (LPA). The bulk electrical conductivities of dried PACA powders in virgin, dedoped and redoped status were measured by a two-disk method with a disk area of 1.00 cm^2 at room temperature using a UT 70A multimeter. The thermostabilities of PACA nanofibrils were measured on a NETZSCH STA 449F3TG-DSC simultaneous thermal analyzer at a temperature range from room temperature to 1000 °C with a heating rate of 20 °C/min in nitrogen. Nitrogen adsorption/desorption measurements at 77.4 K were performed after degassing the PACA powders under high vaccum at 100 °C for at least 20 hours using a DZF-6030A vacuum drying oven. The specific surface areas were calculated by applying the Brunauer–Emmett–Teller (BET) model to adsorption or desorption branches of the isotherms (N_2 at 77.4 K).

2.4 Lead ion adsorption

The metal ion adsorption experiments were carried out according to the methods previously reported.[21] Typically, 40 mg of virgin doped PACA nanofibrils were added to 25 mL of Pb(II) solution at an initial concentration of 10 mmol/L, and the mixture was

then magnetically stirred for 24 h in a water bath at 20 °C. After adsorption, the mixture was filtered and the concentration of Pb(II) remained in the filtrate solution was determined by inductively coupled plasma atomic emission spectrometer (ICP–AES). The adsorbed amount of Pb(II) on the nanofibrils was calculated according to Formula (1) and (2), where Q (mg/g) is the adsorption capacity, q (%) is the adsorptivity, C_0 (mol/L) and C (mol/L) are the lead ion concentrations before and after adsorption, respectively, V (mL) is the initial volume of the lead ion solution, M (g/mol) is the molecular weight of the metal ions, and W (g) is the weight of the nanofibrils added.

$$Q = \frac{(C_0 - C)MV}{W} \quad (1)$$

$$q = \frac{C_0 - C}{C_0} \times 100 \quad (2)$$

3. Results and discussion

3.1 Synthesis of PACA nanofibrils

Selection of polymerization media. Screening of media is of great importance to the chemically oxidative polymerization.[22,35] Solubility experiments show that ACA can be dissolved very well in DMF, DMSO, $C_6H_5NO_2$, $C_6H_4Cl_2$, CH_3NO_2, $CHCl_3$ and $MeCO_2Et$, and DMF and DMSO can also dissolve the common oxidants such as $FeCl_3$, CrO_3, etc. used for the polymerization of AQ monomers.[21,22,36] Note that DMF and DMSO are miscible with acidic water, but $C_6H_5NO_2$, $C_6H_4Cl_2$, CH_3NO_2, $CHCl_3$ and $MeCO_2Et$ are not. In theory, single-phase solvents such as DMSO, DMF as well as biphasic systems including $C_6H_5NO_2/H_2O$, $C_6H_4Cl_2/H_2O$, CH_3NO_2/H_2O, $CHCl_3/H_2O$ and $MeCO_2Et/H_2O$ can be media for polymerization. When DMSO and DMF were used, the oxidative polymerization of ACA indeed occurred, but the polymerization yield and conductivity of the resulting products are very low (see Table 1). Considering that the organic solvents, such as $C_6H_5NO_2$, $C_6H_4Cl_2$, CH_3NO_2, $CHCl_3$ and $MeCO_2Et$ are able to dissolve ACA monomers well, and acidic water can dissolve most common oxidants, it is more worthy to explore the biphasic systems mentioned above as polymerization media. Initially, we judged the polymerization *via* color changes of the reaction. No obvious reaction was observed when $CHCl_3/H_2O$ and $MeCO_2Et/H_2O$ were used. When $C_6H_4Cl_2/H_2O$ was used, the color of organic layer changed from orange-red to brown and then to brownish black within 30 min upon adding CrO_3 oxidant solution into the ACA monomer solution. When $C_6H_5NO_2/H_2O$ and CH_3NO_2/H_2O were used, the color of organic layer changed from brown-yellow to black immediately and the black particles appeared at the interface, indicating that the polymerization of ACA could be induced readily. Note that the virgin PACA particles prepared from $C_6H_5NO_2/H_2O$ biphase exhibit atropurpureus shiny appearance, good conductivity of 8.7×10^{-6} S/cm and high polymerization yield of 38.7%. The solubility tests indicate that the solubilities of ACA in the organic solvents follow the order: $CHCl_3$ (7.9 g/L) < $MeCO_2Et$ (8.6 g/L) < CH_3NO_2 (12.7 g/L) < $C_6H_4Cl_2$ (18.2 g/L) < $C_6H_5NO_2$ (43.9 g/L). On the one hand, the highest solubility of $C_6H_5NO_2$ leads to the monomer and oxidant touch better making the reaction easier. On the other hand, the open-circuit potential (OCP) measurements indicate that the OCPs (*vs.* Ag/AgCl) of ACA in the organic solvents follow the order: CH_3NO_2/H_2O (-297 mV), $C_6H_5NO_2/H_2O$ (-218 mV) < $MeCO_2Et/H_2O$ (-196 mV) < $C_6H_4Cl_2/H_2O$ (-177 mV) < $CHCl_3/H_2O$ < (-148 mV). Both CH_3NO_2 and $C_6H_5NO_2$ effectively reduced the OCP of ACA due to the strong interaction formed between the solvent and the monomer. Lower OCPs could make the aromatic monomers easier to be oxidized and thereby dramatically speed the polymerization reaction.[35] Since both solubility and OCP could be optimized by an appropriate solvent combination such as $C_6H_5NO_2/H_2O$, and $C_6H_5NO_2$ could be recycled after simple separation from biphasic medium through vacuum distillation and drying, we conclude that the $C_6H_5NO_2/H_2O$ is best medium for the ACA polymerization despite of some toxicity of $C_6H_5NO_2$.

Screening of the oxidant species. Variety of oxidants including $FeCl_3$, Br_2, $HClO_4$, K_2CrO_4, CrO_3, NaClO, $KMnO_4$, H_2O_2 and $(NH_4)_2S_2O_8$ with different standard reduction potentials (RP) (see Table 2), were explored to polymerize ACA monomers. It is found that polymerization yield and conductivity of products significantly depends on RP of oxidants. Low RP of oxidants such as $FeCl_3$, Br_2 and $HClO_4$ were too weak to polymerize ACA monomers, producing negligible products. Higher RP (1.20—2.01 V) of oxidants such as K_2CrO_4, CrO_3, NaClO, $KMnO_4$, H_2O_2 and $(NH_4)_2S_2O_8$ were strong enough to initiate polymerization, leading to lots of dark precipitates. Note that the CrO_3 with a moderate RP (1.35 V) is the best oxidant to initiate the polymerization because the product showed the highest yield of 38.7% and conductivity of 8.7×10^{-6} S/cm. Since the residual hexavalent chromium in aqueous layer can readily turn into safe trivalent chromium when treated with ethanol, the use of chromium trioxide will not cause obvious hazard to the natural environment.[37,38] Interestingly, low yield and conductivity were observed when the highest RP (2.01 V) of $(NH_4)_2S_2O_8$ was used as the oxidant. The reason may be that over oxidation of ACA monomers caused by $(NH_4)_2S_2O_8$, produced many soluble oligomers in organic layer and then were easily washed off during the purification.

Optimization of the ACA concentrations and CrO_3/ACA molar ratios. The significant dependence of the polymerization yield and conductivity on the ACA monomer concentrations is showed in Fig. 1a. As the ACA concentrations increased from 25.7 to 142.9 mmol/L in $C_6H_5NO_2/H_2O$, the yield increased dramatically from 38.7 to 56.5%, then kept ignorable changes with further increasing the ACA concentration to 175.0 mmol/L. The virgin PACA synthesized in $C_6H_5NO_2/H_2O$ exhibited the highest conductivity of 9.6×10^{-6} S/cm when the ACA concentration of 142.9 mmol/L was applied. The influence of CrO_3 oxidant/ACA monomer molar ratios on the polymerization yield and conductivity is shown in Fig. 1b. It can be seen that the polymerization yield increased rapidly from 20.1 to 56.5% with increasing CrO_3/ACA molar ratios from 0.5 to 2.0. Further increasing CrO_3/ACA molar ratio changed a little of the polymerization yield. Few reaction active centers will be created at low monomer concentrations and CrO_3/ACA molar ratios, while growth of polymeric chains is easier to be terminated with high monomer concentrations and CrO_3/ACA molar ratios, explaining why the highest conductivity (9.6×10^{-6} S/cm) and good product yield (56.5%) of PACA was obtained at the moderate ACA concentration (142.9 mmol/L) and CrO_3/ACA molar ratio (2.0).

Table 1 Effect of media on the OCPs of ACA, polymerization yields, conductivities, polymer color and maximal wavelengths of virgin PACA salts prepared with an initial ACA concentration of 25.7 mmol/L and a CrO_3/ACA molar ratio of 2.0 in 50 mmol/L of $HClO_4$ single-phase systems and biphasic systems (organic solvent: water = 6:1, v/v) at 30 °C for 72 h.

polymerization medium	single-phase system		biphasic system				
	DMF	DMSO	$MeCO_2Et$ /H_2O	$CHCl_3$ /H_2O	CH_3NO_2 /H_2O	$C_6H_4Cl_2$ /H_2O	$C_6H_5NO_2$ /H_2O
OCP[a] of monomer solution (mV)	–	–	-196	-148	-297	-177	-218
polymerization yield (%)	6.8	3.5	6.5	10.3	34.7	12.8	38.7
electrical conductivity (S/cm)	3.4×10^{-8}	3.9×10^{-7}	1.2×10^{-7}	5.5×10^{-7}	4.3×10^{-6}	6.9×10^{-6}	8.7×10^{-6}
polymer color	brown	brown	brownish black	black	black	black	shiny atropurpureus
λ_{max}(nm)[b]	490	491	489	600	601	606	610

[a] OCP (*vs.* Ag/AgCl): open-circuit potential; [b] λ_{max}: maximal absorption wavelength.

Table 2 Effect of oxidant species on the polymerization yield, bulk electrical conductivity, polymer color and maximal UV-vis absorption wavelength (λ_{max}) of virgin PACA salts prepared with an initial ACA concentration of 25.7 mmol/L and an oxidant/ACA molar ratio of 2.0 in a 50 mmol/L of $HClO_4$ biphasic system consisting of $C_6H_5NO_2/H_2O$ (6:1, v/v) at 30 °C for 72 h.

oxidant (RP[a], V)	$FeCl_3$ (0.77)	Br_2 (1.09)	$HClO_4$ (1.19)	K_2CrO_4 (1.20)	CrO_3 (1.35)	NaClO (1.49)	$KMnO_4$ (1.68)	H_2O_2 (1.77)	$(NH_4)_2S_2O_8$ (2.01)
synthetic yield (%)	1.3	0	0	10.9	38.7	15.4	13.3	14.3	6.1
electrical conductivity (S/cm)	1.5×10^{-8}	–	–	1.1×10^{-8}	8.7×10^{-6}	6.2×10^{-6}	7.4×10^{-9}	6.6×10^{-9}	5.0×10^{-7}
polymer color	black	–	–	brownish black	shiny atropurpureus	black	brown	brown	black
λ_{max}(nm)[b]	645	–	–	591	610	605	491	467	597

[a] RP: standard reduction potential; [b] λ_{max}: maximal UV-vis absorption wavelength.

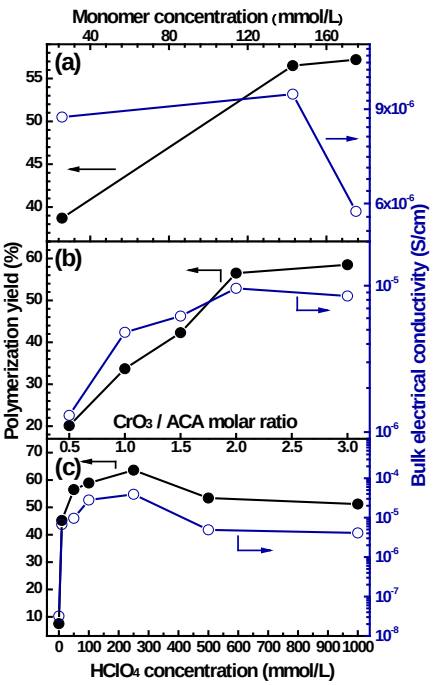

Fig. 1 Dependence of polymerization yield and bulk electrical conductivity of PACAs synthesized in a biphasic system of $C_6H_5NO_2/H_2O$ (6:1, v/v) at 30 °C for 72 h on (a) different initial ACA monomer concentrations at a fixed CrO_3/ACA molar ratio of 2.0 in a 50 mmol/L of $HClO_4$ solution, (b) different CrO_3/ACA molar ratios at a fixed initial ACA concentration of 142.9 mmol/L in a 50 mmol/L of $HClO_4$ solution, and (c) different $HClO_4$ concentrations at a fixed initial ACA concentration of 142.9 mmol/L with a CrO_3/ACA molar ratio of 2.0.

Optimization of $HClO_4$ concentration. Since the ACA monomers can be protonated by proton acid forming ACA amine cations, the addition of acid into the reaction should definitely affect the polymerization procedures. The effect of $HClO_4$ concentrations on the polymerization yield and conductivity of PACAs is shown in Fig. 1c. It is found that the PACA displayed a maximal yield of 63.6% and highest conductivity of 3.9×10^{-5} S/cm when 250 mmol/L of $HClO_4$ was applied. The polymerization can be proceeded in a $HClO_4$-free $C_6H_5NO_2/H_2O$ because of the presence of a small amount of chromic acid produced by the reaction of CrO_3 with water. In the $HClO_4$-free $C_6H_5NO_2/H_2O$ system, the oxidizability of CrO_3 was very weak and no active polymerization sites of aryl amine cations were created, the as-synthesized PACAs exhibited very low polymerization yield of 7.5% and conductivity of 3.2×10^{-8} S/cm. However, when concentrated $HClO_4$ (1.0 mol/L) was introduced, the polymer chains formed would undergo degradation by acidolysis, the PACAs displayed a relatively low polymerization yield (51.2%) and conductivity (4.1×10^{-6} S/cm). This explains why a moderate concentration (250 mmol/L) of $HClO_4$ gave the highest yield (63.6%) and best conductive property (3.9×10^{-5} S/cm).

Optimization of the polymerization temperature. As can be seen in Fig. 2a, with elevating polymerization temperatures from 20 to 50 °C, the PACAs exhibited maximal polymerization yields and conductivities at 20 °C no matter of the status of the polymers (virgin salt, base and redoped salt). Too high temperature would induce drastic chain termination whereas too low temperature might cause low speed of polymerization and less monomer initiation. This explains why a moderate temperature of 20 °C is the optimal temperature for the synthesis of PACA.

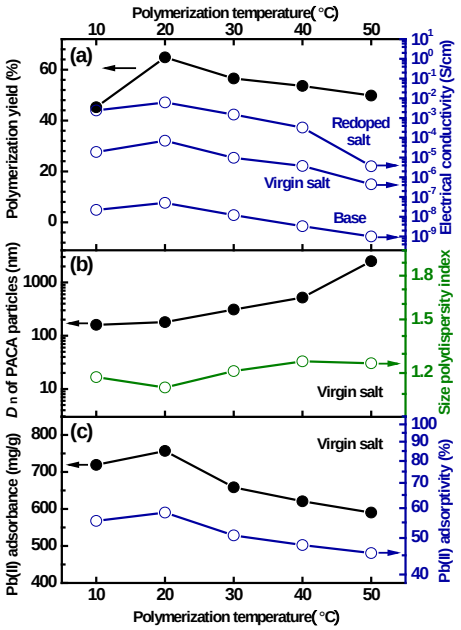

Fig. 2 Effect of polymerization temperatures on (a) the polymerization yield and electrical conductivity of the virgin salt, base and 1.0 mol/L of $HClO_4$ redoped PACAs, (b) the number-average diameter (D_n) and size polydispersity of virgin PACA salt particles, and (c) adsorption capacity and adsorptivity of Pb(II) of PACA polymers. The PACA polymers were synthesized with an initial ACA concentration of 142.9 mmol/L and a CrO_3/ACA molar ratio of 2.0 in a 250 mmol/L of $HClO_4$ biphasic system of $C_6H_5NO_2/H_2O$ (6:1, v/v) at different temperatures for 72 h.

3.2 Chemical structure of PACA nanofibrils

FT-IR spectra. The FT-IR spectra of the ACA monomer and PACA polymers obtained at different polymerization temperature are displayed in Fig. 3. The spectral features of PACAs are similar to those of PAQ oxidized by CrO_3.[22] Strong doublet bands at ~ 3450 and 3333 cm^{-1} owing to $–NH_2$ stretching vibration appear in the spectrum of the ACA monomer. They turned into a broad singlet band centered at ~ 3450 cm^{-1} in the spectra of the PACAs, suggesting that free $–NH_2$ groups in monomers have been converted into –NH– groups after polymerization. The PACAs exhibited (1) a band at 1634 cm^{-1} related to the C=O stretching vibration of the quinone groups; (2) two bands at 1578 and 1491 cm^{-1} associated with the in-plane vibrations of a skeleton of quinoid and benzenoid rings, respectively; (3) a band at 1240 cm^{-1} attributed to the C–N stretching vibration; (4) a broad band at 1196–1050 cm^{-1} assigned to the C–H in-plane deformation vibrations; and (5) two bands at 837–796 and 757–731 cm^{-1} generated from out-of-plane bending vibrations of two and three neighboring C–H groups in benzene rings, respectively. Note that the absorption bands at 1578 and 1491 cm^{-1} in the spectra of the polymers became much more intensive due to the formation of extended conjugation lengths.[39] In the meantime, a moderate band at ~ 706 cm^{-1} in the spectrum of the ACA monomers owing to C–Cl stretching vibration became weaker after polymerization, probably due to the aromatic polymer chains created impaired the p-π conjugation existing in C–Cl bonds, indicating that the oxidative products are real polymers rather than a simple complex or mixture of monomers with some oligomers. Furthermore, the presence of quinoid structures containing C=N bonds signifies that the polymers were created *via* a head-to-tail coupling, i.e., C(4)–N(1) coupling. Briefly, all the PACAs exhibited close characteristics of IR absorption, indicating similar coupling occurred upon altering the polymerization temperature. Note that higher intensity ratios of peaks at 1578 over 1491 cm^{-1} (A_{1578}/A_{1491}) are observed on the PACAs synthesized at low temperatures (10-20 °C) compared to the polymers synthesized at high temperatures (30–50 °C) (0.741–0.744 *vs.* 0.518–0.644). This implies that more quinoid structures and longer polymer chains were created at low temperatures, which is in good accordance with corresponding polymers having higher conductivities as discussed above.

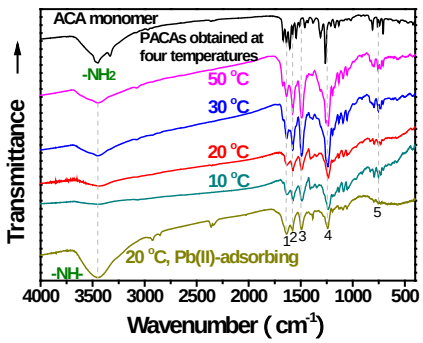

Fig. 3 FT-IR spectra of ACA monomer and PACA polymers prepared with an initial ACA concentration of 142.9 mmol/L and a CrO_3/ACA molar ratio of 2.0 in a 250 mmol/L of $HClO_4$ biphasic system of $C_6H_5NO_2/H_2O$ (6:1, v/v) at different temperatures for 72 h.

UV–vis spectra. Fig. 4 shows the normalized UV–vis absorption spectra of the ACA monomer and PACA polymers obtained in DMF. Both ACA monomer and PACAs exhibited a strong absorption at ~265 nm due to the π–π* transition within benzene rings. The monomers displayed a weak absorption band at 481 nm, originating from the n–π* transition of the anthraquinone moieties. Most of PACAs exhibited a new strong and broad band at 591–611 nm associated with an intra-molecular charge transfer of the entire large π–conjugated polymers. It is found that the UV-vis maximal absorbance wavelengths (λ_{max}) and their intensities significantly depended on the polymerization media. The UV–vis spectra of PACAs prepared in DMF, DMSO and $MeCO_2Et/H_2O$ showed the shortest λ_{max} at 490 nm, whereas PACA obtained in $C_6H_5NO_2/H_2O$ displayed the longest λ_{max} at 610 nm, as showed in both Fig. 4a and Table 1. Certainly, $C_6H_5NO_2/H_2O$ would be the best medium for the formation of PACAs with the longest conjugation length as well as highest yield and conductivity. Meanwhile, it is observed from Fig. 4b that the intensity ratio of the exciton bands at 610 nm over 265 nm ($I_{610\ nm}/I_{265\ nm}$) increased steadily upon changing of oxidant from H_2O_2 to $KMnO_4$, $FeCl_3$, K_2CrO_4, $(NH_4)_2S_2O_8$, NaClO and CrO_3 in the biphasic system of $C_6H_5NO_2/H_2O$. This is well agreed with the changes of conductivity, as listed in Table 2. The highest $I_{610\ nm}/I_{265\ nm}$ of PACA synthesized with CrO_3 exhibited the highest conductivity and polymerization yield as well as the longest conjugation length.

With alternating reaction parameters, as-synthesized PACAs exhibited highest $I_{610\ nm}/I_{265\ nm}$ values of 0.481, 0.481, 0.505 and 0.542, if using 142.9 mmol/L of monomer concentration, 2.0 of CrO_3/ACA molar ratio, 250 mmol/L of $HClO_4$ and 20 °C of polymerization temperature, respectively, as showed in Fig. S1. In summary, the optimal synthetic conditions for PACAs as following: oxidant, CrO_3; medium, 250 mmol/L $HClO_4/C_6H_5NO_2$ (1:6, v/v); temperature, 20 °C; CrO_3/ACA molar ratio, 2.0 and polymerization time, 72 h.

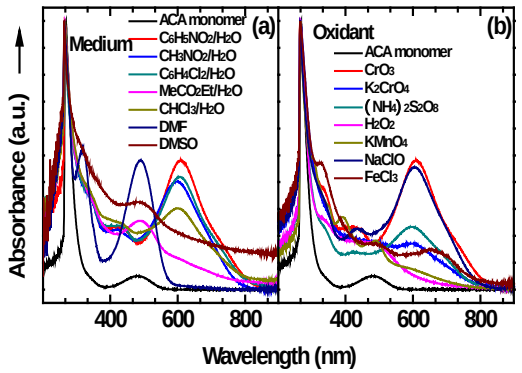

Fig. 4 Normalized UV–vis absorption spectra of ACA monomer and PACAs prepared with (a) a CrO_3/ACA molar ratio of 2.0 in the 50 mmol/L $HClO_4$ single-phase systems and biphasic systems (organic solvent : water = 6:1, v/v), and (b) an oxidant/ACA molar ratio of 2.0 in a 50 mmol/L $HClO_4$ biphasic system of $C_6H_5NO_2/H_2O$ (6:1, v/v) with an initial ACA concentration of 25.7 mmol/L at 30 °C for 72 h.

Wide-angle X-ray diffractograms. The wide-angle X-ray diffractograms of ACA monomer and PACA powders obtained at different polymerization temperature are showed in Fig. 5. All of these PACAs displayed a broad diffraction peak centered at 22.5–25.9°, and a very weak diffraction around 7.6°, 12.2°, or 16.0°. The two peaks centered at 12.2 and 22.5–25.9° should be attributed to the periodicity perpendicular and parallel to the polyaniline-like main chains, respectively.[40,41] As compared to the highly crystalline ACA monomers, PACAs showed substantially amorphous structures or most partly crystalline structures and are similar with their polymer analogues such as poly(5-sulfo-1-aminoanthraquinone) (PSA) and poly(1-aminoanthraquinone) (PAQ).[21,22] PACAs obtained at a relatively low polymerization temperature appeared to be more amorphous, whereas PACA obtained at a higher polymerization temperature (50 °C) exhibited some crystallinity. The reason may be that the latter polymers have relatively low molecular weight (i.e., shorter molecular chains) as indicated by MALDI/TOF mass spectra (Fig. 6b, c), while shorter molecular chains are favorable for the formation of ordered or oriented PACA salt crystals. In fact, the relatively high crystallinity of the PACA salts obtained at higher temperature (50 °C) has been further confirmed by their relatively strong endothermicity due to the crystallite melted at 304 °C, as seen in Fig. 11. However, the amorphous structures could favor the penetration and then adsorption of heavy metal ions into the PACA nanofibrils because the macromolecular chains in the amorphous states are relatively looser than those in the crystalline states (see details below).

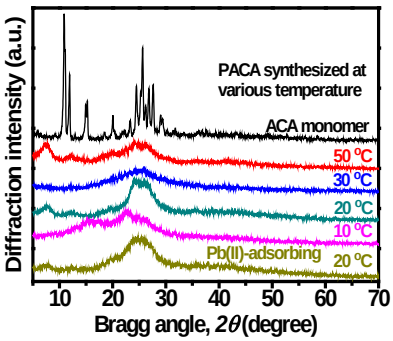

Fig. 5 WAXD diffractograms of ACA monomer, PACA salts prepared at various temperatures with an initial ACA concentration of 142.9 mmol/L and a CrO_3/ACA molar ratio of 2.0 in a 250 mmol/L $HClO_4$ biphasic system of $C_6H_5NO_2/H_2O$ (6:1, v/v) for 72 h, and PACA salt after adsorption of Pb(II) ions in the $Pb(NO_3)_2$ aqueous solution (25 mL) at the initial metal ion concentration of 10 mmol/L at 20 °C with 40 mg of adsorbent for 24 h.

MALDI/TOF mass. The MALDI/TOF mass spectra (Fig. 6) show that the PACA salts have a wide polymer chain length distribution. The molecular weight, i.e., the polymerization degree of PACAs significantly depended on the polymerization temperature and oxidant species applied. The polymerization degrees were found to be 4–10 and 9–15 when PACAs were synthesized with NaClO and CrO_3 at 20 °C (Fig. 6a,b), respectively. When CrO_3 was used as oxidant, PACAs synthesized at 20 °C exhibited a high molecular weight up to 5886. The proportion of high molecular weight PACA-containing components decreased with increasing polymerization temperature from 20 to 50 °C. Additionally, most mass numbers are attributed to quasi-molecular ions or metal ion adducts since chlorine atoms, oxygen atoms, and amino/imino groups have a strong affinity with H^+, K^+ or other cations in the matrix or environment. It should also be noted that the calculated mass differential (Δm) between some quasi-molecular ions and their corresponding theoretical molecules with the same polymerization degree, is about 36.5, a value exactly equivalent to the mass of HCl. Interestingly, this phenomemon appeared only when NaClO was used as the oxidant (see Fig. 6a). This is because the reduction product (HCl) from NaClO is easy to be doped in virgin PACAs.

3.3 Size distribution, morphology and surface area of PACA nanofibrils

Conventional micro-emulsion and dispersion polymerization routes for preparation of nanostructured conducting polymers require a large number of external stabilizer or emulsifier. In this study, unexpected fine nanofibrils of PACA polymers were readily obtained by an interfacial chemical oxidative polymerization in an acidic biphasic medium with no need of any external stabilizer or emulsifier. The size and morphology of the PACA nanofibrils made with NaClO and CrO_3 were analyzed by TEM technique and laser particlesize analysis, as shown in Figs. 2, 7. The TEM images show that the PACA nanofibrils appear to gather into clusters with belt-like (Fig. 7a–d) and bamboo leaf-shaped (Fig. 7e–f) morphologies. Large amounts of nanofibrils

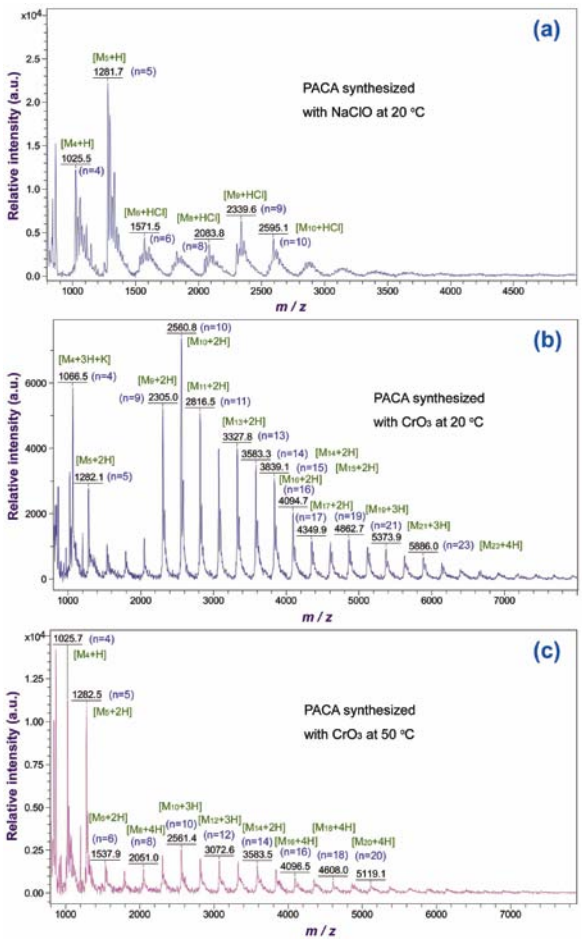

Fig. 6 MALDI/TOF mass spectra of PACA salts prepared at an initial ACA concentration of 142.9 mmol/L in a 250 mmol/L of $HClO_4$ biphasic system of $C_6H_5NO_2/H_2O$ (6:1, v/v) with a oxidant/ACA molar ratio of 2.0 and with the oxidant (a) NaClO at 20 °C; (b) CrO_3 at 20 °C; and (c) CrO_3 at 50 °C for 72 h.

interpenetrate with each other forming single nanofibril bundles with diameters of 20–70 nm, lengths of 0.2–3 μm and aspect ratios of 10–100. Notably, the longest nanofibrils were obtained if NaClO was used as an oxidant with an initial ACA concentration of 25.7 mmol/L (Fig. 7a, b). These nanofibrils have a diameter of around 10 nm and a length of around 1–3 μm and seem to interpenetrate with each other forming nanofibril bundles with diameters of around 20–70 nm. With increasing ACA concentrations from 25.7 to 142.9 mmol/L, the lengths of PACA nanofibril bundles decrease from several micrometers to < 1 μm and the aspect ratios also decrease apparently, when NaClO was used as the oxidant. The aspect ratios of the nanofibrils thus depended on the monomer molar concentration, which is consistent with the results from a dilute polymerization method to make polyaniline and oligotriphenylene nanofibers.[28,42] During dilute polymerization, a large amount of PACA was able to be continuously deposited onto the active nuclei resulting in bulk quantities of nanofibers with high aspect ratios. This is in contrast to the polymerization using a high concentration of monomer in which a large number of polymers readily form and precipitate, followed immediately by secondary growth leading to shorter and bigger diameters of nanofbrils. Interestingly, oxidant species also played a noticeable role in altering the morphology of PACA nanostructures. When the NaClO oxidant was replaced by CrO_3, belt-like PACA nanofibrils tuned to bamboo leaf-shaped clusters. The *ca.* average diameters and lengths of the nanofibrils decreased from 40 to 30 nm and 0.8 to 0.3 μm, respectively. Note that the redox potentials (E_{ox}) of $NaClO/H^+$ and CrO_3/H^+ are calculated to be 1.49 and 1.35 V, respectively. Lower redox potential of oxidants are used, smaller diameters of the nanofibrils are readily formed,[14,43] explaining why smaller diameters of nanofbrils were obtained using CrO_3 as oxidant.

The PACA nanofibrils were further characterized by LPA and BET measurements. The diameters (D_n) of PACA nanofibrils increased upon increasing polymerization temperature from 10 to 50 °C (160–2500 nm), but the polydispersity index (PDI) is the lowest (1.13) when the polymerization reaction was carried at 20 °C. The low PDIs further confirm that uniform PACA nanofibrils have been created. The PACA nanofibrils synthesized at different temperature were used as representative examples to investigate the surface area of the nanofibrils, which could be important for applications such as sensors and heavy metal ion adsorbents. The BET surface areas of nanofibrils are calculated to be 29, 33, 30, 27 and 25 m^2/g when the PACAs were synthesized at 10, 20, 30, 40 and 50 °C, respectively. The PACAs nanofibrils synthesized under optimal conditions exhibited the highest surface area (i.e., free volume) of 33 m^2/g.

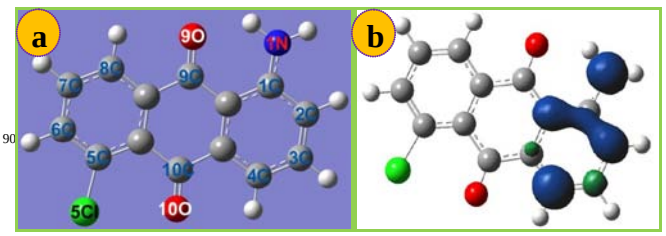

Scheme 1 (a) Molecular model of ACA with minimized energy; (b) Isovalent surfaces (0.004 electron/bohr^3) of spin electron density (in blue) in ACA.

3.4 Polymerization mechanism of ACA

To get deep insight into PACA structures and the polymerization mechanism, the atomic electron density population, the proportion of frontier orbitals and atomic electron spin density of the ACA monomer (Scheme 1a) were calculated at the B3LYP/6-31G (*d*) level using Gaussian 09 software (Table S1). The results reveal that the main negative electron charges locate on C(2), C(3), C(4), C(6), C(7), C(8), N(1), O(9) and O(10), implying that these atoms can donate electrons and then form radical cations easily upon treating with oxidants.[44–46] According to the molecular orbital theory, the reaction between active molecules occurs mainly on the frontier molecular orbitals and neighboring orbitals. In the case of ACA, the proportions of atoms in the highest occupied molecular orbital (HOMO) (Table S2) follow the order: N(1) > C(4) > C(2) >> O(9) > O(10) > C(3) > C(6) = C(8) > Cl(5) > C(7). That is to say, N(1), C(4) and C(2) atoms would be more negatively charged. Taking the effect of steric hindrance into account, the coupling polymerization would occur preferentially at N(1) and C(4) positions. Besides, electron spin

density (ESD) would be another important factor determining the possibility of oxidative polymerization coupling.[47,48] The ESD of ACA monomer radical cations was calculated at the B3LYP/6-31G (*d*) level, as listed in Table S3. Meanwhile, the isovalent surfaces of the ESD of the ACA monomer are shown in Scheme 1b. The results indicate that the N(1), C(4) and C(2) atoms display the highest ESD and the values follow the order: C(2) < C(4) < N(1), further signifying that C(4)–N(1) coupling occurred during chemical oxidative polymerization.

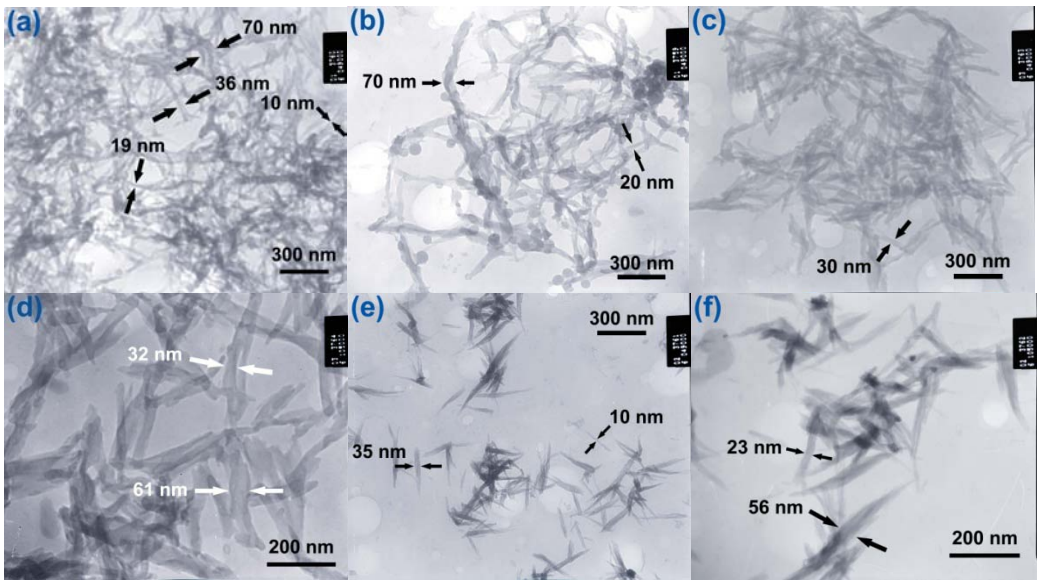

Fig. 7 (a–d): TEM images of PACA nanofibrils prepared with an initial ACA concentration of 25.7 mmol/L (a–b) and 142.9 mmol/L (c–d) and a NaClO/ACA molar ratio of 2.0 in a 250 mmol/L $HClO_4$ biphasic system of $C_6H_5NO_2/H_2O$ (6:1, v/v) at 20 °C for 72 h; (e–f): TEM images of PACA nanofibrils prepared with an initial ACA concentration of 142.9 mmol/L and a CrO_3/ACA molar ratio of 2.0 in a 250 mmol/L $HClO_4$ biphasic system of $C_6H_5NO_2/H_2O$ (6:1, v/v) at 20 °C for 72 h.

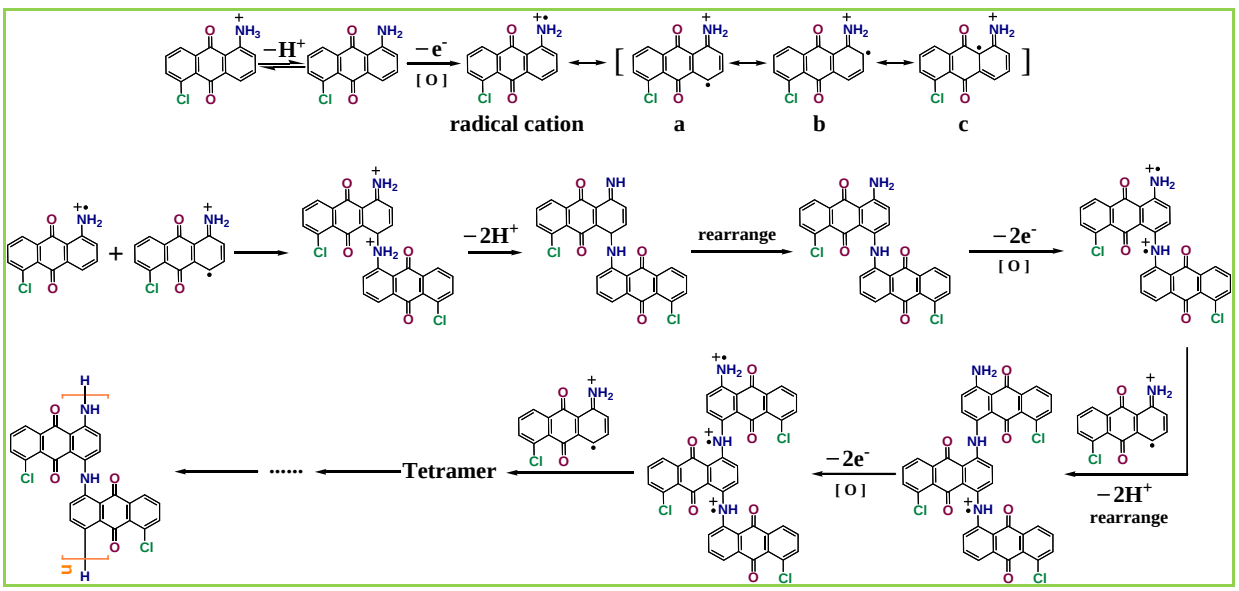

Scheme 2 Proposed polymerization mechanism of ACA.

Based on FT-IR, MALDI/TOF mass spectra and theoretical calculations, one could logically conclude that chemical oxidative polymerization of ACA took place most likely through the head-to-tail coupling between the *para*-position C(4) and the oxidizable amino group. This is well coincidence with the chemical oxidative polymerization coupling mechanism of aniline proposed by Nicolas-Debarnot *et al.*[45,49] Therefore, the polymerization mechanism of ACA can be proposed, as illustrated in Scheme 2. The initial step would be forming the radical cation through an electron transfer from ACA nitrogen atom to the oxidant. The radical cation of monomer has three resonance forms, among which the form (a) is the more reactive

one due to its high substituent inductive effect and low steric hindrance. The next step would be the reaction occurred between the radical cation and the resonance form (a), i.e., so-called "head-to-tail" coupling, which is usually favored by acidic medium, forming the dication dimer and then becoming neutral dimer after deprotonation and rearrangement. The dimer could be oxidized easier than the monomer and able to form a new biradical dication immediately. Then the formed biradical dication dimer could couple with either radical cation monomer or itself, affording trimers and tetramers, respectively, eventually leading to the ACA polymers upon undergoing growth of polymer chains.

3.5 Formation mechanism of self-stabilized PACA nanofibrils

The ACA monomer is readily soluble in the $C_6H_5NO_2$ phase but not in the aqueous phase (see Fig. 8a), and CrO_3 oxidant behaviors reversely (see Fig. 8b). The monomer would meet the oxidant mainly at the interface between the $C_6H_5NO_2$ and aqueous phases. By vigorously stirring the biphasic mixture, the aqueous phase would form a large amount of small microdroplets. The stability of the microdroplets formed in nitrobenzene primarily determined by their interfacial tension and interaction as well as mechanical stirring. Because of the interfacial tension, the small microdroplets could likely merge into the aqueous phase once they formed. Fortunately, the water is partially compatible with nitrobenzene owing to hydrogen-bonding interaction existing between hydroxyl and nitro groups. Therefore, ACA monomer at the boundary between nitrobenzene and aqueous phase tended to form an ammonium salt *via* protonation and thus enhancing the miscibility of hydrophilic microdroplets and hydrophobic nitrobenzene. In addition, the protonated ACA monomers, i.e., ACA ammonium cations themselves would self-assemble into micelles surrounding the aqueous phase owing to the hydrophilic ammonium cations and hydrophobic anthraquinone groups. These micelles could stabilize the microdroplets formed and acted as soft templates for self-assemblies of nanostructures. In the meantime, the number of aqueous microdroplets formed in nitrobenzene phase, to a great extent, could be maintained by vigorously stirring because homogeneous miniemulsion was created. Once the CrO_3 oxidant and the protonated ACA monomer molecules contacted at biphasic interface, the PACA polymer chains would be immediately created. Due to the high rigidities and strong π-π interactions existing among the ACA molecules,[22,50] the growth of polymer chains was limited along one-dimension direction and finally self-assembled into PACA nanofibrils in the aqueous microdroplets, as depicted in Fig. 9 and Fig. 10a. Furthermore, negatively charged PACA nanofibrils would rapidly diffuse into the organic phase upon vigorously stirring (≥ 300 rpm) because of the water-insoluble nature of the polymers, thus ensuring the interface fresh always until the monomers were completely consumed.

PACA nanofibrils can be easily dispersed in water upon 10 minute sonication. The dispersion is very stable and no precipitates are found upon standing for 24 h. The excellent self-stabilization of PACA nanofibrils is likely attributed to the static repulsion effect resulted from negatively charged surfaces of the nanofibrils, as indicated by theoretical energy calculation. The atomic electron density population of an energy-minimized molecular model of ACA decamer (see Fig. 10b) was calculated at the B3LYP/6-31G (*d*) level using Gaussian 09 software (see Table S4). The results show that the nitrogen-atoms and oxygen-atoms are more negatively charged than other atoms. Surprisingly, the chlorine-atoms in PACAs are slightly positively charged, probably caused by the p–π conjugation existing between the chlorine atoms and anthraquinone rings. Therefore, the existence of naked oxygen-atoms on the anthraquinone rings, together with nitrogen-atoms in polymer main chains, would be responsible for the surface negatively charged nanofibrils. A statical repulsion among the as-formed nanofibrils avoids secondary growth or overgrowth of polymers stack on the nanofibrils primarily formed. This explains why small diameters, excellent dispersibility and self-stability of nanofibrils could be created. The negatively charged quinone groups acting as internal stabilizers for PACA nanofibrils is further confirmed by adding electrolytes such as NaCl into the their water-dispersion. Upon adding 0.5 and 0.8 mol/L NaCl electrolytes into the nanofibrils water-dispersion, the particles were precipitated entirely within 24 h and 2 h (Fig. S2), respectively. This is in contrast with the PACA nanofibrils are highly stable in water for 24 h without adding of electrolytes.

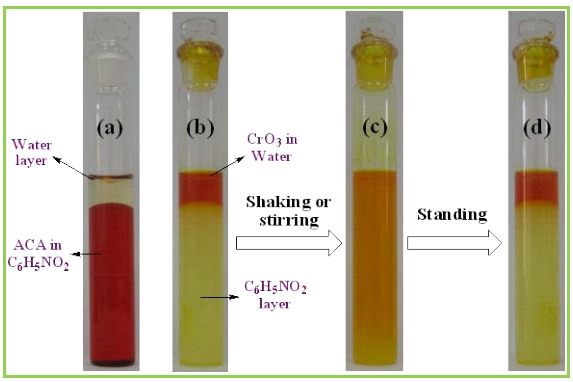

Fig. 8 (a) Distribution of ACA in the two immiscible phases; (b–d) Formation and gradual disappearing of CrO_3 aqueous miniemulsion in nitrobenzene after respective vigorous shaking or stirring and standing for a little while.

3.6 Properties of PACA nanofibrils

Chemical resistance. As summarized in Table S5, PACA nanofibrils are weakly soluble in THF and partly soluble in DMF, NMP and DMSO, whereas the ACA monomers are completely soluble in above solvents. However, both PACA nanofibrils and ACA monomers are completely insoluble in water, 0.5 mol/L of HCl and 0.5 mol/L of NaOH. All the PACA solutions show same color of dark cyan no matter what solvents were used.

Thermostability. As can be seen from Fig. 11, thermogravimetric (TG) and differential thermogravimetric (DTG) curves of PACAs exhibited two stages of thermal degradation at below 100°C and 450–520 °C because of water elimination and main chain decomposition of the polymers, respectively, which coincide with the corresponding endothermic temperatures indicated by DSC. The residues of PACAs at 1000 °C are as high as 58–61%, equivalent to 88.2–92.8% of the theoretical carbon content (65.7%). The PACA obtained at 20 °C showed the highest initial decomposition temperature (520 ^{o}C) and residue at 1000 ^{o}C (61%), thanks to its highest conjugation. Differential

scanning calorimetry (DSC) scans of PACAs synthesized at 10, 20 and 50 °C displayed a weak endothermic peak centered at 50–78 °C due to the evaporation of 2–4% water trapped inside the polymers, and very weak endothermic peaks at 273, 273 and 304°C, respectively, probably originating from the melting of small part of ACA oligomers. The formation of a shiny black block of coke after heating to 1000 °C (see Fig. S3) suggests a melting process of the original polymer powders has indeed occurred. Besides, the strong and broad endothermic peaks centered at 487, 515 and 517 °C, respectively, were observed for PACAs obtained at 10, 20, and 50 °C, ascribing to the pyrolysis of the main chains of the PACAs. The excellent thermostability of PACA nanofibrils is most likely owing to the high aromaticity and rigidity of the polymer skeleton structures. The PACAs nanofibrils would be suitable precursors for making carbon nanomaterials as well as heat-resisting metal-ion-adsorbents (see details below).

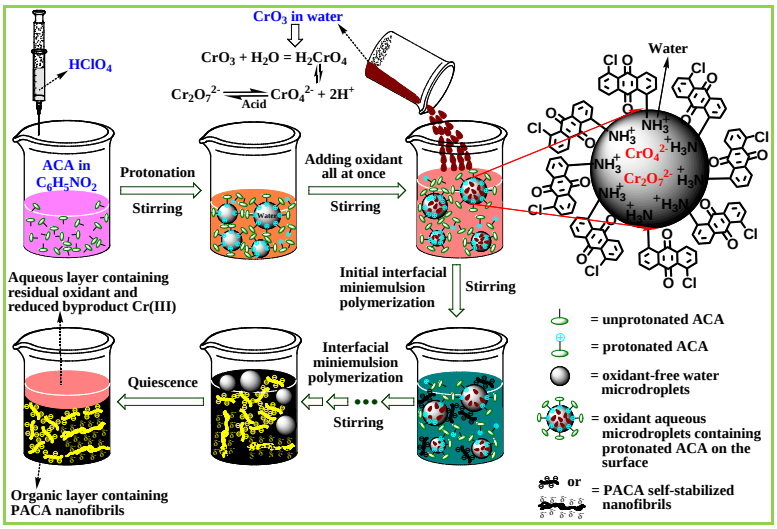

Fig. 9 Possible formation and self-stabilized mechanisms of PACA nanofibrils synthesized in the biphasic system of $C_6H_5NO_2/H_2O$.

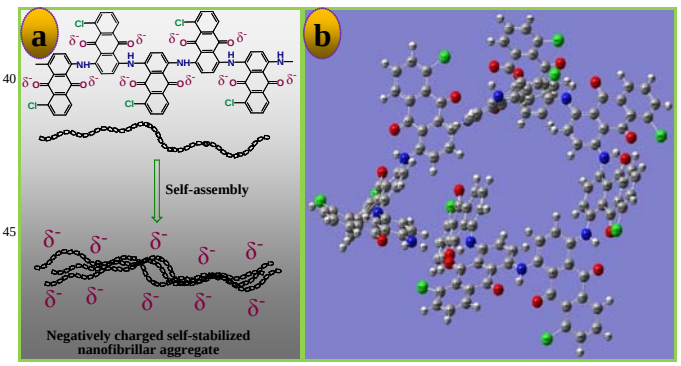

Fig. 10 (a) Formation of negatively charged self-stabilized nanofibril aggregation; (b) Molecular model with minimized energy of negatively charged self-stabilized PACA with 10 repeat units according to the result of MALDI/TOF mass spectra; the blue, red, green, big gray and small gray balls represent nitrogen atoms, oxygen atoms, chlorine atoms, carbon atoms and hydrogen atoms, respectively.

Bulk electrical conductivity. The bulk electrical conductivity of the PACA polymers can be simply tuned between 1.0×10^{-9} and 6.2×10^{-3} S/cm by controlling synthetic conditions and doping levels, as shown in Tables 1, 2 and Figs. 1, 2a. The conductivity of virgin PACA salts increases steadily with changing polymerization media from DMF, $MeCO_2Et/H_2O$, DMSO, $CHCl_3/H_2O$, CH_3NO_2/H_2O, $C_6H_4Cl_2/H_2O$, to $C_6H_5NO_2/H_2O$ (Table 1) or oxidant from H_2O_2, $KMnO_4$, K_2CrO_4, $FeCl_3$, $(NH_4)_2S_2O_8$, NaClO, to CrO_3 (Table 2). Besides, the maximal conductivities of PACAs could be optimized by altering monomer concentrations (9.6×10^{-6} S/cm), oxidant/monomer molar ratios (9.6×10^{-6} S/cm), $HClO_4$ concentrations (3.9×10^{-5} S/cm) and polymerization temperature (7.1×10^{-5} S/cm). The conductivity of PACA nanofibrils synthesized at the optimal conditions could be further improved >150 times (3.9×10^{-5} *vs.* 6.2×10^{-3} S/cm) through dedoping and then redoping by NH_4OH and $HClO_4$, respectively. Note that, upon heating to 1000 °C, derived-carbon materials exhibited 10 and 3 magnitudes increase in conductivity compared to precursors of dedoped (1.0×10^{-9} *vs.* 38 S/cm) and redoped (6.2×10^{-3} *vs.* 38 S/cm) PACA nanofibrils, respectively.

Fluorescence properties. The fluorescent excitation and emission spectra of the ACA monomer and PACA nanofibrils synthesized with the two oxidants at different initial ACA concentration are shown in Fig. 12. PACAs and ACA monomers exhibited close excitation and emission spectra with similar shape and peaks. All excitation spectra show a triplet band in the range of 300−390 nm owing to $\pi\rightarrow\pi^*$ electronic transitions found in both anthraquinone amine monomers and their polymers.[21,22,36] All the emission spectra generated by the radiative decay of excitons, have more pronounced vibronic structures, and exhibit a maximal peak at 410−420 nm, indicating PACA nanofibrils are typical blue-light emitting materials. Note that, with a same concentration (6.0 μg/mL), PACA nanofibrils prepared under optimal conditions displayed twice emission intensity in comparison with the ACA monomers most likely due to the much

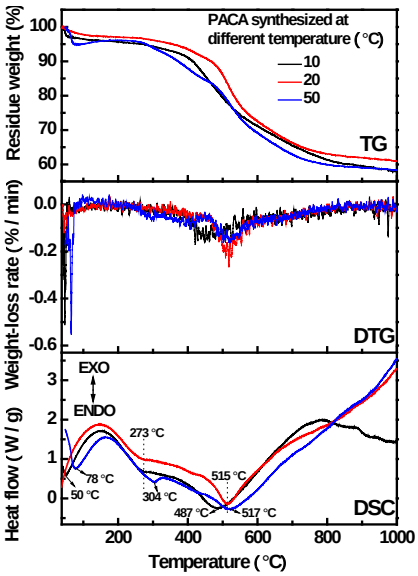

Fig. 11 TG, DTG and DSC curves of dedoped PACAs prepared with an initial ACA concentration of 142.9 mmol/L and a CrO_3/ACA molar ratio of 2.0 in a 250 mmol/L of $HClO_4$ biphasic system of $C_6H_5NO_2$/H_2O (6:1, v/v) at different temperatures for 72 h.

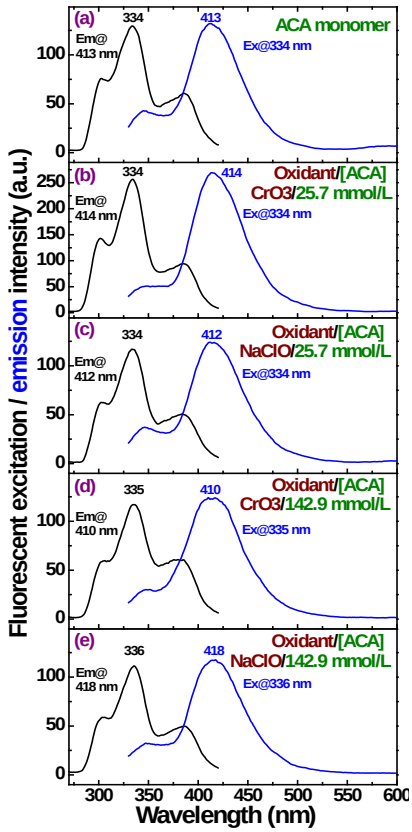

Fig. 12 Fluorescent excitation and emission spectra obtained at fixed slit widths of 5 nm of 6.0 μg/mL ACA and PACA solutions in DMF. The PACAs were prepared with an oxidant/monomer molar ratio of 2.0 in 50 mmol/L $HClO_4$ biphasic system of $C_6H_5NO_2$/H_2O (6:1, v/v) at 30 °C for 72 h.

improved π-conjugation and tactic chains observed in polymers.[21] As calculated by Gaussian software above, PACAs are high negatively charged because of the contribution of electron-rich groups including –NH–, –N═, –NH_2, ═O, and –Cl bearing in polymer chains. This allows PACAs as promising materials for electron-deficient ions sensing *via* fluorescence quenching, as exampled by our recent report.[51]

Lead-ion adsorption. Thanks to the electron-rich, negatively charged surface, high free volume and stability, PACA nanofibrils could be used for heavy metal ions adsorbents. In our case, Pb(II) was used for model heavy metal ion to investigate the possibility. As shown in Fig. 2c, the adsorption capability and adsorptivity of Pb(II) display maximal values of 756.8 mg/g and 58.4%, respectively, when optimal PACA nanofibrils were used as adsorbents. The Pb(II) adsorption ability (756.8 mg/g) of PACA nanofibrils is very competitive with some good results observed on poly(1-aminoanthraquinone) nanofibrils (95.8 mg/g),[22] polysulfoaminoanthraquinone nanoparticles (89.6 mg/g),[21] polyphenylenediamine nanoparticles (89.0 mg/g),[52] *m*PD/SPD copolymer microparticles (91.8 mg/g),[53] and polyaniline/rice bran composite (30.11 mg/g),[11] when some concentration of Pb(II) ion is used.

The PACA nanofibrils synthesized at 20 °C exhibited best adsorption for Pb(II) with increasing the polymerization temperature from 10 to 50 °C, most likely attributed to the highest surface area and free volume as well as the longest polymer chains (i.e., existence of a large amount of adsorption sites such as–N═, –NH–, –NH_2, C═O and –Cl), as discussed above. The Pb(II) adsorption was further confirmed by the FT-IR and WAXD spectra (Figs. 3, 5). FT-IR spectra indicate that the band at 3450 cm^{-1} (–NH– stretching) became broader and the band at 1634cm^{-1} (C═O stretching) shifted to 1637 cm^{-1}as well as both peaks became much more intensive, most likely resulted by the strong interaction between the Pb(II) ion and the PACA nanofibrils. Upon Pb(II) treatment, the WAXD spectra of PACA nanofibrils show a weaker diffraction at 7.6°, and a 0.6° shift of the strongest diffraction peak at 24.1° owing to the Pb(II) ion adsorption onto the PACA nanofibrils. Additionally, Pb(II) ions could exchange with the protonated –N═, –NH–, –NH_2 and C═O cations allowing a high adsorption capacity. Actually, the pH of Pb(II) solution obviously decreased by 0.64 after treated by the nanofibrils (4.05 *vs.* 3.41) because of the release of H^+ ions through the ion exchanges, further implying the ion exchanges occurred.

4. Conclusions

Water-dispersible and self-stabilized poly(1-amino-5-chloroanthraquinone) (PACA) nanofibrils have been successfully synthesized *via* a facile interfacial chemical oxidative polymerization without any external stabilizer. Reaction media, oxidant species, monomer concentrations, oxidant/monomer molar ratios, acid concentrations and temperatures were optimized for the formation of uniform PACA nanofibrils with a high polymerization yield, tunable size and electrical conductivity, good chemical resistance, high thermostability, strong blue-light emitting fluorescence as well as high Pb(II) adsorption. The FT-IR and MALDI/TOF mass spectra as well as theoretical

calculations showed that high molecular weight of PACAs were created *via* the "head-to-tail" coupling of the monomer at N(1) and C(4) positions. The high negatively charged surface of PACA chains generated from quinone groups is the driving force to formation of polymer nanofibril bundles with diameters of 20–70 nm, high water-dispersibility and self-stability. PACA nanofibrils exhibit tunable conductivity ranging from 1.0×10^{-9} to 38 S/cm upon simply regulating the polymerization conditions, acid-doping/base-dedoping as well as thermal treatment. Most importantly, PACA nanofibrils can be excellent adsorbents for lead ions, the adsorption capacity is as high as 756.8 mg/g, which are very competitive with most good Pb(II)-sorbents previously reported. With these impressive functionalities, PACA nanofibrils are promising for target applications such as water-treatment, sensors, electrodes and precursors for making carbon nanomaterials.

Acknowledgements

This work was supported by the National Natural Science Foundation of China (Grant Nos. 51363012 and 51203090), the Marie Curie International Incoming Fellowship (No. 326385), the Natural Science Foundation of Shanghai (12ZR1446700) and Kunming University of Science and Technology (Projects KKSY201232041, 2014ZX01, 2014ZX03 and 2014ZX05).

Notes and references

[a] *Research Center for Analysis and Measurement, Kunming University of Science and Technology, Kunming, 650093, China. Fax: +86-871-65111617; Tel: +86-871-65113971; E-mail: huangshaojun1975@163.com*
[b] *School of Chemistry, University of Bristol, Bristol, England BS8 1TS, UK. E-mail: yaozu.liao@gmail.com*
[c] *State Key Laboratory of Theoretical and Computational Chemistry, Institute of Theoretical Chemistry, Jilin University, Changchun, 130023, China*
[d] *School of Materials Science and Engineering, University of Shanghai for Science and Technology, Shanghai, 200092, China*

† Electronic Supplementary Information (ESI) available: Main atomic electron density populations for ACA, main composition and proportion of frontier orbitals in ACA, main atomic electron spin densities for ACA, main atomic electron density populations for PACA, solubility and solution color of ACA and PACA, normalized UV–vis absorption spectra of PACAs, dispersions of the PACA nanofibrils upon adding NaCl electrolyte, and pictures of ACA, PACA and carbon residue. See DOI: 10.1039/b000000x/

1 J. Han, L. Wang and R. Guo, *J. Mater. Chem.*, 2012, **22**, 5932.
2 J. Han, J. Dai, L. Li, P. Fang and R. Guo, *Langmuir*, 2011, **27**, 2181.
3 J. Han, L. Y. Li and R. Guo, *Macromolecules*, 2010, **43**, 10636.
4 J. Han, Y. Liu and R. Guo, *J. Am. Chem. Soc.*, 2009, **131**, 2060.
5 S. Marx and A. Baiker, *J. Phys. Chem. C*, 2009, **113**, 6191.
6 S. Guo, S. Dong and E. Wang, *Small*, 2009, **5**, 1869.
7 C. C. Huang, T. C. Wen and Y. Wei, *Mater. Chem. Phys.*, 2010, **122**, 392.
8 J. Tian, S. Liu and X. Sun, *Langmuir*, 2010, **26**, 15112.
9 W. Yan, X. Feng, X. Chen, W. Hou and J. J. Zhu, *Biosens. Bioelectron.*, 2008, **23**, 9.
10 Y. B. Jiang and C. X. Kuang, *Mini-Rev. Med. Chem.*, 2013, **13**, 713.
11 F. Kanwal, R. Rehman, J. Anwar and M. Saeed, *Asian J. Chem.*, 2013, **25**, 2399.
12 A. N. Aleshin, *Adv. Mater.*, 2006, **18**, 17.
13 J. Han, P. Fang, J. Dai and R. Guo, *Langmuir*, 2012, **28**, 6468.
14 H. Ding, M. Wan and Y. Wei, *Adv. Mater.*, 2007, **19**, 465.
15 J. Huang and R. B. Kaner, *Chem. Commun.*, 2006, **28**, 367.
16 Y. Z. Liao, V. Strong, W. Chian, X. Wang, X. G. Li and R. B. Kaner, *Macromolecules*, 2012, **45**, 1570.
17 H. A. A. El-Rahman and J. W. Schultze, *J. Electroanal. Chem.*, 1996, **416**, 67.
18 M. S. Won, W. H. Yoon and Y. B. Shim, *Electroanalysis*, 2005, **17**, 1952.
19 J. A. Freire, G. A. Dal Moro, R. Toniolo, I. A. Hummelgen and C. A. Ferreira, *Org. Electron.*, 2006, **7**, 397.
20 M. Skompska, M. J. Chmielewski and A. Tarajko, *Electrochem. Commun.*, 2007, **9**, 540.
21 M. R. Huang, S. J. Huang and X. G. Li, *J. Phys. Chem. C*, 2011, **115**, 5301.
22 X. G. Li, H. Li, M. R. Huang and M. G. Moloney, *J. Phys. Chem. C*, 2011, **115**, 9486.
23 Z. Y. Tang and G. X. Xu, *Acta Phys.-Chim. Sin.*, 2003, **19**, 307.
24 G. X. Xu, L. Qi, L. Wen, G. Q. Liu and Y. X. Ci, *Acta Polym. Sin.*, 2006, **6**, 795.
25 R. Li, Z. Chen, J. Li, C. Zhang and Q. Guo, *Synth. Met.*, 2013, **171**, 39.
26 P. Singh and R. A. Singh, *Synth. Met.*, 2012, **162**, 2193.
27 S. Xing, H. Zheng and G. Zhao, *Synth. Met.*, 2008, **158**, 59.
28 Y. Z. Liao, V. Strong, Y. Wang, X. G. Li, X. Wang and R. B. Kaner, *Adv. Funct. Mater.*, 2012, **22**, 726.
29 J. Stejskal, I. Sapurin and M. Trachova, *Prog. Polym. Sci.*, 2010, **35**, 1420.
30 B. Gupta and R. Prakash, *Synth. Met.*, 2010, **160**, 523.
31 N. Nuraje, K. Su, N. I. Yang and H. Matsui, *ACS Nano*, 2008, **2**, 502.
32 J. Li, Q. Jia, J. Zhu and M. Zheng, *Polym. Int.*, 2008, **57**, 337.
33 W. Li, M. Zhu, Q. Zhang and D. Chen, *Appl. Phys. Lett.*, 2006, **89**, 103110.
34 E. N. Konyushenko, J. Stejskal, I. Sedenkova, M. Trchova, I. Sapurina, M. Cieslar and J. Prokes, *Polym. Int.*, 2006, **55**, 31.
35 X. G. Li, J. Li, Q. K. Meng and M. R. Huang, *J. Phys. Chem. B*, 2009, **113**, 9718.
36 X. G. Li, H. Li and M. R. Huang, *Chem. Eur. J.*, 2007, **13**, 8884.
37 J. Li, P. Jin and C. Tang, *RSC Adv.*, 2014, **4**, 14815.
38 S. Tiwari, S. N. Singh and S. K. Garg, *Biorem. J.*, 2014, **18**, 158.
39 A. I. Drachev, A. B. Gil'man and A. A. Kuznetsov, *High Energ. Chem.*, 2005, **39**, 418.
40 X. G. Li, J. L. Zhang and M. R. Huang, *Chem.Eur. J.*, 2012, **18**, 9877.
41 H. K. Chaudhari and D. S. Kelkar, *J. Appl. Polym. Sci.*, 1996, **62**, 15.
42 F. Ferri, M. Greco, G. Arcovito, M. De Spirito and M. Rocco, *Phys. Rev. E*, 2002, **66**, 011913.
43 G. Li, L. Jiang and H. Peng, *Macromolecules*, 2007, **40**, 7890.
44 X. G. Li, M. R. Huang, W. Duan and Y. L. Yang, *Chem. Rev.*, 2002, **102**, 2925.
45 D. Nicolas-Debarnot and F. Poncin-Epaillard, *Anal. Chim. Acta*, 2003, **475**, 1.
46 N. Gospodinova and L. Terlemezyan, *Prog. Polym. Sci.*,1998, **23**, 1443.
47 S. Ando and M. Ueda, *Synth. Met.*, 2002, **129**, 207.
48 J. Doskocz, M. Doskocz, S. Roszak, J. Soloducho and J. Leszczynski, *J. Phys. Chem. A*, 2006, **110**, 13989.
49 A. I. Drachev, A. B. Gil'man, E. S. Obolonkova and A. A. Kuznetsov, *Synth. Met.*, 2004, **142**, 35.
50 M. Adachi and M. Harada, *Langmuir*, **2000**, **16**, 2376.
51 S. Huang, P. Du, C. Min, Y. Liao, H. Sun and Y. Jiang, *J. Fluoresc.*, 2013, **23**, 621.
52 X. G. Li, R. R. Zhang and M. R. Huang, *J. Comb. Chem.*, 2006, **8**, 174.
53 M. R. Huang, H. J. Lu and X. G. Li, *J. Mater. Chem.*, 2012, **22**, 17685.

